PCCP

PAPER

View Article Online
View Journal | View Issue

Cite this: *Phys. Chem. Chem. Phys.*, 2017, **19**, 29449

The influence of particle size of amino-functionalized MCM-41 silicas on CO_2 adsorption†

G. Gatti,[a] C. Vittoni,[a] D. Costenaro,[a] G. Paul,[a] E. Mangano,[b] S. Brandani,[b] L. Marchese[a] and C. Bisio *[ac]

Received 31st July 2017,
Accepted 18th October 2017

DOI: 10.1039/c7cp05177h

rsc.li/pccp

The CO_2 adsorption properties of hybrid organic–inorganic MCM-41 silicas with different particle sizes are described here. Micrometric to nanometric MCM-41 silicas are functionalized by introducing amino groups *via* grafting of 3-[2-(2-aminoethyl)aminoethyl]aminopropyltrimethoxysilane (PAPTS). A combination of FTIR and SS-NMR spectroscopies is adopted to distinguish between physisorbed and chemisorbed CO_2. A higher amount of CO_2 is physisorbed in the nanometric sample because of a higher pore volume, whereas chemisorbed (carbamate and acid carbamic) species are more abundant in the micrometric sample. The adsorption process is also quantitatively studied using three different techniques (*i.e.* volumetric measurements, Thermo-Gravimetric Analysis (TGA) and Zero Length Column (ZLC) analysis), especially focusing on the reversibility of the reactions between CO_2 and amino groups. The three techniques show a higher CO_2 adsorption capacity for MCM-41 with nanometric size compared to the micrometric one. Finally, the process is studied at different temperatures (*i.e.* from 35 to 90 °C) in order to find the best operating conditions.

Introduction

Due to the increasing energy demand required to meet the technological needs of society, in the last few years growth of anthropogenic CO_2 emissions has been registered. This phenomenon leads to global climate change effects, such as the increase of the global temperature, which are harmful for the entire ecosystem.[1] In this scenario, it becomes necessary to decrease the amount of CO_2 emitted to the atmosphere. For these reasons, CO_2 capture methods have attracted great attention, due to their potential to sequester large amounts of carbon dioxide from concentrated sources, such as power plants.[2] Traditional CO_2 capture technologies include adsorption by using liquid solutions of amines. However, this process presents several problems, mainly related to the corrosion of the apparatus, the volatility of the employed solutions and the high amount of energy required for the sorbent regeneration.[3]

In the last two decades, numerous studies have investigated CO_2 adsorption using solid adsorbents such as activated carbons, hydrotalcites, metal oxides, zeolites, hybrid organic–inorganic materials, metal organic frameworks and porous polymers, in a wide range of pressures and temperatures.[4,5] These materials can be physical or chemical adsorbents. Porous carbons, zeolites and metal organic frameworks belong to the class of physisorbent materials, while hydrotalcites, metal oxides and hybrid organic inorganic materials containing basic species belong to the class of chemisorbent materials. In fact, in such solids CO_2 is retained because of chemical reactions.

CO_2 capture using physical sorbents requires less energy during the adsorption compared to processes based on chemical adsorption. This is mainly due to the fact that in physisorption-based processes no covalent bonds are formed, therefore, less energy is required for the adsorbent regeneration.[6] In addition, for physisorbent materials the adsorption capacity rapidly decreases upon increasing the temperature.[7]

Considering the typical stack temperatures of a power plant, the adsorbers should preferably operate in a range from room temperature to 150 °C: using chemical adsorption, such as in materials containing amino groups, allows operation at the higher range of these temperatures. In this case, CO_2 can react chemically with amino groups, forming ammonium carbamates and carbamic acid.[8]

Many types of hybrid organic–inorganic materials containing amino-groups have been reported in the literature;[9–12] these

[a] *Dipartimento di Scienze e Innovazione Tecnologica and "Centro interdisciplinare Nano-SiSTeMI", Università del Piemonte Orientale, via T. Michel 11, 15121, Alessandria, Italy. E-mail: chiara.bisio@uniupo.it*
[b] *Scottish Carbon Capture and Storage, School of Engineering, University of Edinburgh, Mayfield Road, Edinburgh, EH9 3JL, UK*
[c] *ISTM-CRN Istituto di Scienze e Tecnologie Molecolari, via G. Venezian 21, Milano, Italy*

† Electronic supplementary information (ESI) available. See DOI: 10.1039/c7cp05177h

have been obtained mainly through grafting or impregnation of different organic molecules on inorganic supports.[13]

In particular, there are many examples of amino groups introduced in mesoporous silica, as reported by Xu *et al.* In that work, the authors developed and tested a PEI-modified MCM-41 silica, which is a "molecular basket" for CO_2 in the condensed form.[14] In particular, a synergistic effect of the mesoporous molecular sieves and the PEI on the adsorption of CO_2 was observed. A CO_2 adsorption capacity of 215 mg g^{-1}-PEI at 75 °C was obtained. This value is 24 times higher than that of pure MCM-41 and even 2 times higher than that of the pure PEI. Unfortunately, in the hybrid materials obtained by impregnation, the amino groups are physisorbed onto the support and suffer from a lack of stability after several cycles.[15] With this regard, alternative synthesis routes using organic–inorganic materials obtained by grafting of amino-silane have the potential to enhance the long-term stability of this class of materials.[16]

In the present study we focus on the design of MCM-41 adsorbents containing amino groups *via* grafting of 3-[2-(2-aminoethyl)aminoethyl]aminopropyltrimethoxysilane (PAPTS). This silane was selected following our previous study on SBA-15 silicas functionalised with 3-aminopropyltriethoxysilane (APTS), 3-(2-aminoethyl) aminopropyltrimethoxysilane (EAPTS) and 3-[2-(2-aminoethyl)aminoethyl] aminopropyltrimethoxysilane (PAPTS). From this study it was evident that samples containing a higher amount of amino groups in the chain are more reactive, following the order PAPTS > EAPTS > APTS, and for this reason we decided to use PAPTS as a grafting agent for MCM-41 samples.[17]

The effect of the adsorbent particle size on the CO_2 adsorption properties is an interesting aspect not widely investigated in the literature. For example, Meis *et al.*[18] studied the size effects of hydrotalcites. In their work they found that the CO_2 adsorption capacity significantly increases upon decreasing the LDH particle size. Furthermore, studies on the size effect of zeolites on carbon dioxide adsorption have been performed by Galhotra *et al.*[19] In particular they found that nanosized zeolites show different sites for CO_2 adsorption on the surface with respect to microsized ones.

In order to study the size effect of the support on hybrid organic–inorganic materials, MCM-41 with a particle diameter from the micrometric to nanometric scale has been studied. Adsorption of CO_2 on these samples was monitored using different techniques. FT-IR spectroscopy was employed to distinguish between physisorption and chemisorption processes. These results were compared to solid state NMR spectroscopy results, which are also able to provide a semi-quantitative estimation of the physisorbed and chemisorbed fractions of CO_2 in the grafted samples.

Volumetric measurements, Thermo-Gravimetric Analysis (TGA) and Zero Length Column (ZLC) analyses were also adopted to study quantitatively the adsorption–desorption process, with a special focus on the reversibility of the reactions.

Additional hints were obtained from the CO_2 adsorption measurements at different temperatures (35 to 90 °C).

Experimental

Material preparation

MCM-41 silicas. In order to obtain MCM-41 silica with micrometric size, cetyl trimethylammonium bromide (CTAB, 15.12 g, Sigma Aldrich, ≥98%) was dissolved in 38 mL of deionized water and then heated at 50 °C. Tetramethylammonium hydroxide (TMAOH, 8.94 mL, Sigma-Aldrich) was then added, and after 30 minutes silica fumed (5.0 g, Aldrich, 99.8%) was introduced. After 1 h the gel was transferred to the Teflon cup (125 mL capacity) of an autoclave (Anton PAAR 4748) and heated in an oven at 120 °C for 72 h. After the hydrothermal treatment, the sample was filtered, washed with 2 L of deionized water and dried for 36 h at 120 °C. The material was calcined under air flow at 600 °C for 5 h in order to remove completely the CTAB template.[20] The sample obtained will be hereafter named MCM-41 micro.

Nanosized mesoporous MCM-41 particles were prepared following a method previously reported in the literature.[21] Cetyl trimethylammonium chloride (CTAC, 2.6 g, Sigma Aldrich, ≥98%) and Pluronic F127 (2.0 g, Sigma Aldrich) were dissolved in a 0.3 M hydrochloric acid solution (30 g, Sigma Aldrich, ≥37%) at room temperature, and tetraethylorthosilicate (TEOS, 3.5 g, Sigma Aldrich) was then added to the solution. After stirring for 3 h, 3.0 g of ammonium hydroxide solution (Riedel-de Haën, 33%) was introduced. The gel obtained was aged by stirring at room temperature for 24 h and then heated in a thermostatic bath at 60 °C for 24 h. The sample obtained was filtered, washed with distilled water and then dried at room temperature overnight. The surfactants were finally removed from the sample by calcination at 600 °C in air flow for 3 h with a ramp temperature of 1 °C min^{-1}. The sample obtained will be hereafter named MCM-41 nano.

Functionalization with amino groups. Both MCM-41 silica samples were functionalized with *N*-[3-(trimethoxysilyl)propyl]-diethylenetriamine (PAPTS, Sigma-Aldrich, 97%) using a post-synthesis grafting method in order to introduce amino groups on the silica surface. Before functionalization, 1.0 g of MCM-41 silica was treated under vacuum at 200 °C for 2 h in order to remove physisorbed water. After this treatment, the sample was kept under N_2 flow and then dispersed in a solution of 100 mL of anhydrous toluene (Sigma Aldrich, 99.8%) and 0.48 mL of PAPTS was slowly added drop-by-drop. The dispersion was then kept under magnetic stirring for 20 h at 50 °C. Finally, the sample was recovered by filtering, and the powder was dried at 80 °C overnight after washing with toluene and diethyl ether (Sigma Aldrich, ≥98%) to remove the unreacted silane.[22]

The obtained samples were hereafter named P_MCM-41 micro and P_MCM-41 nano.

Characterization techniques

TEM micrographs. TEM micrographs were collected on a JEOL 2010 High Resolution Transmission Electron Microscope operating at 300 kV. Specimens were prepared by sonicating the sample in isopropanol and by depositing a drop of the suspension on carbon-coated grids.

X-ray diffractrograms (XRD). X-ray diffractrograms (XRD) were collected on unoriented ground powders using a Thermo ARL 'XTRA-048 diffractometer with CuKα (λ = 1.54 Å) radiation, from 2 and to 7° 2θ degrees with a step size of 0.02° 2θ and a rate of 1° 2θ min^{-1}.

N_2 physisorption measurements. N_2 physisorption measurements were carried out at 77 K in the relative pressure range from 10^{-7} to 1 P/P_0 using a Quantachrome Autosorb iQ2 volumetric system. Before the analysis the samples were outgassed at 135 °C for 3 h (residual pressure $p < 10^{-7}$ Torr). Specific surface areas were determined using Brunauer–Emmett–Teller (BET) analysis, in the residual pressure range from 0.01 to 0.1 P/P_0. Pore size distributions were obtained by applying the Non Localized Density Functional Theory (NLDFT) method (N_2 silica kernel based on a cylindrical pore model).

C–H–N elemental contents. C–H–N elemental contents were determined using an EA 3000 elemental analyzer (EuroVector). Helium and oxygen at 120 and 35 kPa pressure, respectively, were used. For each material, three measurements were carried out.

Infrared spectra. Infrared spectra were collected on an Equinox 55 Spectrometer (Bruker) (resolution 2 cm^{-1}). Self-supporting pellets were placed into an IR cell with KBr windows permanently attached to the vacuum line (residual pressure: 1.33 × 10^{-4} Pa), allowing all treatments and adsorption–desorption experiments to be carried out *in situ*. The cell is also equipped with a heating system that allows the sample to be kept at a specific temperature during analysis. Before the gas adsorption tests, the silica samples were outgassed at 135 °C for 3 h under dynamic vacuum, using an oil-free apparatus and grease-free vacuum line. The samples were then cooled at the desired temperature for the collection of the IR spectra upon CO_2 adsorption at 35, 50, 70 and 90 °C, respectively. The IR spectra were normalized taking as a reference the intensity of the overtones and combination modes of the silica framework (bands in the 2200–1600 cm^{-1} range). This is because the band intensity related to intrinsic oscillators of the materials is proportional to the amount of such species in the samples. As a result of the normalization, the absorbance values are reported in arbitrary units (a.u.).

Thermogravimetric analysis (TGA). For the determination of the silanol concentration a Setaram Setsys instrument was used. A sample of about 10–15 mg was packed in an alumina crucible, which was counterbalanced by an identical empty crucible. The differential balance measures the difference between the weight of the reference and the sample crucibles. The measurements were done under Argon flow (20 ml min^{-1}) from 20 to 1100 °C (1 °C min^{-1} heating rate). CO_2 adsorption measurements were carried out on a Setaram Sensys Evo TG/DSC apparatus. Typically, for these experiments, a sample mass of *ca.* 20–30 mg was packed in a platinum crucible, which was counterbalanced by an identical platinum crucible packed with an equivalent mass of lead beads. Prior the measurements the sample was pretreated at 135 °C for 3 h (2 °C min^{-1} heating rate) under Helium flow (50 ml min^{-1}). The sample was then cooled to the desired temperature of the experiment (20, 35, 50, 70 and 90 °C) and the adsorption was performed by exposing the sample to a mixture of 10 vol% of CO_2 in He at a constant total flow rate of 50 ml min^{-1} for 2 h. The CO_2 concentration and the adsorption time were chosen to be representative of a typical post-combustion capture process from a coal-fired power plant. Experiments at a higher adsorption time (*i.e.* 6 h of adsorption) were also conducted, but have led to adsorption capacity values comparable to those obtained after 2 hours. For this reason, it was decided to report only the experiments after 2 hours of contact. At the end of the adsorption step the inlet flow is then switched to pure He at the same flow rate for 2 h to allow the desorption of CO_2. In the case of a purely physisorption process, assuming that equilibrium has been achieved and no transport resistances are present, the change in the sample weight in the adsorption and desorption step should be the same, indicating a perfectly reversible process. The CO_2 capture capacity and the heat of adsorption were also calculated.[23] The uncertainty of enthalpy measurement has been evaluated by TG-DSC measuring the melting enthalpy of the Indium wire standard material (purity: 99.995%, melting temperature: 156.598 °C, fusion enthalpy: 28.51 kJ mol^{-1}) and comparing the measured data with the standard. The obtained uncertainty of the enthalpy is less than 1%.

The zero length column (ZLC). The Zero Length Column (ZLC) consists of a 1/8'' Swagelok union in which 10–15 mg of sample are placed as monolayers between two sintering discs. This system can be modified to allow more samples to be packed in the adsorption column (20–40 mg) obtaining an Extended Zero Length Column (E-ZLC). This is approximately three times the length of a traditional ZLC (25.9 mm) and uses a 1/8'' Swagelok bulkhead connector allowing the use of the same apparatus developed for the standard ZLC experiment. The system is equipped with drying columns to ensure the removal of any traces of water from the gases entering the system. The technique is based on following the desorption curve of a sample pre-equilibrated with a known adsorbate concentration. In a typical experiment, after the regeneration at 135 °C under He flow overnight, the sample is equilibrated with a mixture of 10% CO_2 in He at atmospheric pressure and a constant flow rate (adsorption step). Once equilibrium is reached the inlet flow to the column is switched to pure He (purge) at the same flow rate to allow CO_2 to desorb. The concentration in the gas phase is monitored using a Dycor Ametek Benchtop quadrupole mass spectrometer connected to the outlet of the ZLC. A detailed description of the system is provided in a previous publication.[24] The amount of sample packed in the E-ZLC was 26.1 mg and 36.5 mg for P_MCM-41 micro and P_MCM-41 nano respectively. Each experiment was carried out at two different desorption flow rates (2, 2.7 ml min^{-1}) in order to check if the samples are equilibrium or kinetically controlled.[25] Before starting the desorption process, it must be ensured that complete equilibrium is reached: the system is considered at equilibrium when the CO_2 uptake does not change with the increase of the adsorption time. According to this procedure the resulting equilibration time for the P_MCM-41 micro and P_MCM-41 nano samples was 30 min for both. In order to

ensure that all CO_2 adsorbed would be desorbed from the sample, the desorption step at constant temperature (35 °C) was followed by Temperature Programmed Desorption (TPD).[26] By slowly ramping the temperature (from 35 °C to 120 °C at 1 °C min^{-1}) any chemisorbed fraction of CO_2, strongly rooted to the supports, is released.

Volumetric measurements. The CO_2 volumetric measurements were carried out at 35 and 50 °C in the relative pressure range from 10^{-2} to 1000 mbar by using a Quantachrome Autosorb iQ2 instrument. Before the analysis the samples were outgassed at 135 °C for 3 h (1 °C min^{-1} heating rate and residual pressure $p < 10^{-6}$ Torr).

Solid state NMR spectra. Solid state NMR spectra were acquired on a Bruker Avance III 500 spectrometer and a wide bore 11.7 Tesla magnet with operational frequencies for ^{13}C of 125.77 MHz. A 4 mm triple resonance probe with MAS was employed in the experiments. The samples were packed on a Zirconia rotor and spun at a MAS rate between 0 and 15 kHz. The magnitude of radio frequency fields, υ_{rf}, was 62.5 kHz for ^{13}C MAS NMR and the relaxation delay between accumulations was 60 s. Chemical shifts are reported using the δ scale and are externally referenced to TMS at 0 ppm. All ^{13}C MAS NMR spectra were fitted with DMFIT functions for quantitative deconvolution of overlapping peaks.[27] Before the gas adsorption tests, the samples were outgassed at 135 °C with a heating ramp of 1 °C min^{-1} for 3 h using an oil-free apparatus and grease-free vacuum line. The samples were cooled to room temperature and 100 mbar of $^{13}CO_2$ was placed in contact with the samples and then kept in that atmosphere for at least 2 days. The labelled $^{13}CO_2$ was used in order to increase the ^{13}C NMR signal intensity.

Results and discussion

Physico-chemical properties of organo-modified MCM-41 silicas

The diffraction pattern of MCM-41 micro and nano samples (Fig. S1, curves a and b, ESI†) shows reflections located at 2.7, 4.3 and 5.0° 2θ degree, corresponding to the (100), (110) and (200) families of planes, respectively, which are typical of materials with a hexagonal arrangement of ordered cylindrical pores.[17] On the other hand, grafted MCM-41 silica samples (Fig. S1, curves a′ and b′, ESI†) show mainly the basal reflection at 2.4° 2θ degree, indicating that the introduction of the organo-silane decreases the order of the typical structure of the MCM-41 materials. The morphology of MCM-41 silica samples was investigated using transmission electron microscopy (TEM). Typical images of samples obtained are reported in Fig. 1.

The MCM-41 micro sample (Fig. 1A) is composed of micrometric particles with a mean diameter of about 200–300 nm. The ordered arrangement of pores of this sample is clearly visible from the micrograph reported in Fig. 1A. The MCM-41 nano sample (Fig. 1B) preserves the same ordered structure, but the mean diameter of particles is reduced to around 40 nm.[28]

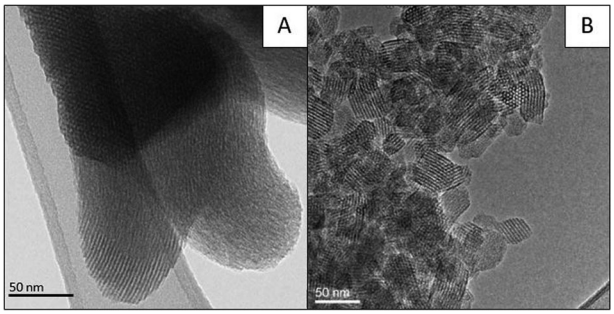

Fig. 1 TEM micrographs of MCM-41 micro (A) and MCM-41 nano silicas (B).

The reduction of the size of the MCM-41 nano sample, compared to MCM-41 micro, is due to the introduction in the synthesis of a second surfactant (Pluronic F127), which avoids the growth of the grains tailoring the size of the silica particles.[18]

The N_2 physisorption analysis at 77 K was performed in order to obtain information on the textural properties of the MCM-41 grafted silicas, with special attention to the determination of the specific surface area and pore size distribution. The N_2 adsorption–desorption isotherms and pore size distribution are reported in Fig. 2.

MCM-41 micro and nano samples (Fig. 2, curves a and b) show type IV adsorption isotherms based on the IUPAC classification, indicating the presence of mesoporosity in the materials.[29] The MCM-41 nano sample presents a hysteresis loop at high P/P_0 values, not observable in the MCM-41 micro sample, due to the aggregation of small particles. After the grafting procedure, the shape of the isotherm is modified. In particular, the volume of adsorbed N_2 decreases in the grafted samples.

The specific surface area (S.S.A), estimated with the BET method, and pore volume values are reported in Table 1. Before the functionalization the specific surface area values are 1205 and 893 $m^2\ g^{-1}$, for MCM-41 micro and nano respectively. After the grafting procedure, the samples show a reduction of the specific surface area with respect to the bare MCM-41 silicas (−70% for both samples), ascribed to the presence of the organic species that limit the access to the pores. Despite P_MCM-41 micro containing about the same amount of amino groups as P_MCM-41 nano (about 1×10^{-2} mmol m^{-2}, see Table 1), the pore volume decreases more (−60% for P_MCM-41 micro, −45% for P_MCM-41 nano), suggesting that for P_MCM-41 micro the amino chains are present mostly inside the pores, while for P_MCM-41 nano species grafted onto the external surface contribute significantly to the overall concentration. This effect should be related to the reduced pore size of MCM-41 nano with respect to MCM-41 micro, that is in part limiting the access of the amino silane into the pores (length of PAPTS chain: 8.9 Å).

The presence of the PAPTS on the surface of the silica particles was monitored using Infrared Spectroscopy (Fig. 3). The FT-IR spectra of the silica samples (Fig. 3, curves a and b) in the high frequency range are characterized by the presence of a main band located at 3745 cm^{-1} and a broad adsorption in

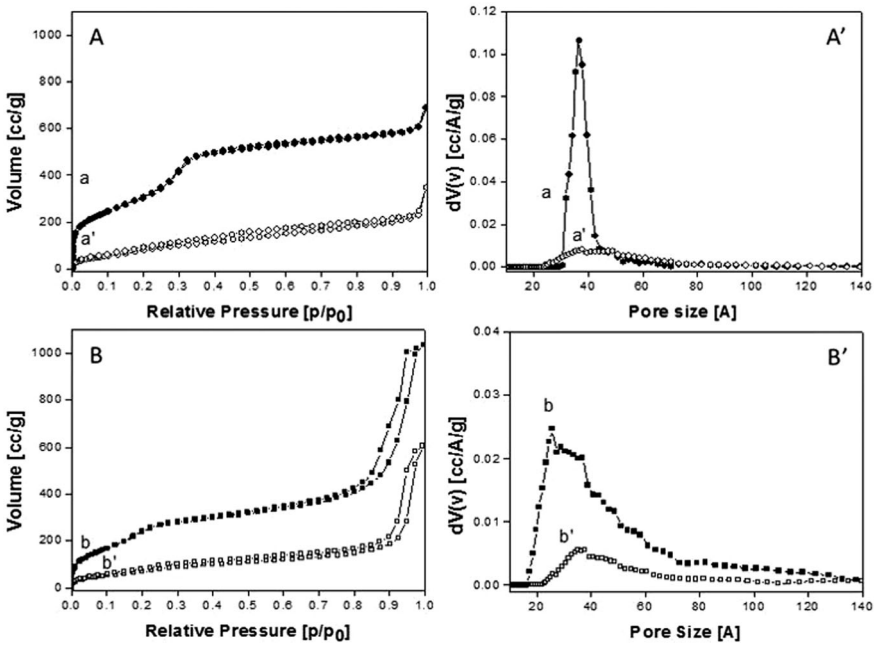

Fig. 2 N_2 adsorption–desorption isotherms at 77 K and relative pressures (P/P_0) from 1×10^{-7} to 1 (sections A and B) and pore size distribution determined using NLDFT methods (sections A′ and B′) of MCM-41 micro (a), P_MCM-41 micro (a′), MCM-41 nano (b) and P_MCM-41 nano (b′).

Table 1 Specific surface area and pore volume values obtained by N_2 physisorption analysis and nitrogen concentration values determined by elemental analysis

Sample	SSA [$m^2\ g^{-1}$]	V_p [$cc\ g^{-1}$]	Conc. N [$mmol\ g^{-1}$]	Conc. N [$mmol\ m^{-2}$]
MCM-41 micro	1205	0.894	—	—
P_MCM-41 micro	372	0.363	3.57	0.95×10^{-2}
MCM-41 nano	893	1.552	—	—
P_MCM-41 nano	268	0.864	3.17	1.1×10^{-2}

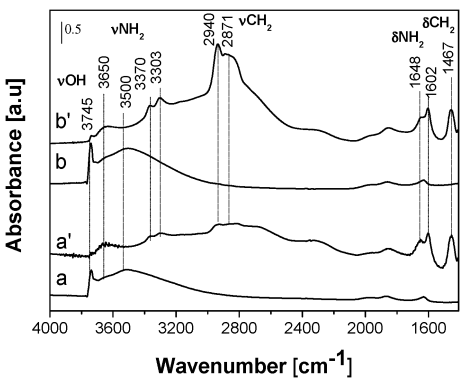

Fig. 3 FT-IR spectra of MCM-41 micro (a), P_MCM-41 micro (a′), MCM-41 nano (b) and P_MCM-41 nano (b′) samples. Spectra were recorded after outgassing of the samples at 100 °C for 1 h in order to remove the physisorbed water.

the 3700–3000 cm^{-1} range, in which bands at *ca.* 3650 and 3500 cm^{-1} can be distinguished. The sharp component at 3745 cm^{-1} is due to the stretching mode of isolated silanol groups, whereas the broad absorption at lower frequencies is ascribed to the stretching mode of H-bonded OH species in weak interaction with each other.[30] It can be noticed that in the MCM-41 nano sample (Fig. 3, curve b) the intensity of the bands is more pronounced compared to the other sample, thus indicating the presence of a greater number of silanols (both isolated and H-bonded) compared to the MCM-41 micro sample (Fig. 3, curve a). This observation is also confirmed by the quantitative determination of the silanol concentration made using TGA analysis that shows 2.78 SiOH nm^{-2} for the MCM-41 micro and 3.16 SiOH nm^{-2} for the MCM-41 nano sample, respectively. The concentration of silanol species has been obtained by using eqn (1), where $\%H_2O$ = water weight loss due to the condensation of SiOH groups, 2 is the number of silanols needed to form a water molecule by condensation, N_A = Avogadro's number (6.022×10^{23}), M.W. H_2O = molecular weight of water (18.01 g mol^{-1}) and S.S.A is the specific surface area estimated by N_2 physisorption analysis.

$$\text{SiOH nm}^{-2} = \frac{\%H_2O}{100 - \%H_2O} \times \frac{2 \times N_A}{\text{M.W.}_{H_2O} \times \text{S.S.A}} \quad (1)$$

Eqn (1): estimation of surface SiOH group concentration.

In the low frequency region, the spectra of both silica samples exhibit absorption bands at *ca.* 1980, 1865 and 1600 cm^{-1}, due to the overtones and combination modes of the silica framework.[31]

As expected, after the grafting procedure (Fig. 3, curves a′ and b′) the bands due to surface SiOH, both isolated and H-bonded, are strongly decreased in intensity due to the fact that these surface species: (i) react with the PAPTS silane and (ii) are H-bonded with the PAPTS amino groups.

The IR spectra of both grafted samples (Fig. 3a′ and b′) are characterized by the presence of complex absorptions in the 3500–2000 cm^{-1} range. The components at 3370 and 3303 cm^{-1}

are due to the asymmetric and symmetric stretching modes of amino groups, respectively, the associated bending mode falling at 1602 cm^{-1}.[30] The band at 1648 cm^{-1} can be associated with the bending mode of the PAPTS NH groups.[30] The bands in the 3000–2800 cm^{-1} range are due to the asymmetric and symmetric stretching modes of CH_2 groups of silane introduced onto the silica surface by the grafting procedure, the associated bending modes falling at *ca.* 1467 cm^{-1}.[30] The broad band extending between 3500 and 2000 cm^{-1} is due to the occurrence of strong H-bonds between the silanols and the PAPTS amino groups, which are bent towards the silica surface.[17]

IR and SS-NMR study of the interaction between CO_2 and organo-modified MCM-41 silica at 35 °C

Infrared spectroscopy of adsorbed carbon dioxide was used to study the interactions between CO_2 and the organo-modified mesoporous silicas. IR spectra collected after the exposure of the hybrid samples to 60 mbar of CO_2 at 35 °C are reported in Fig. 4.

After dosage of 60 mbar of CO_2, the IR spectrum of the P_MCM-41 sample (Fig. 4A, curve a′) appeared strongly modified. In particular, the decrease in intensity of the bands at 3370 and 3303 cm^{-1}, related to the stretching modes of NH_2 groups, indicates the reaction of CO_2 with basic species thus forming ammonium carbamate and carbamic acid.[8] At lower frequencies, bands due to both physisorbed and chemisorbed CO_2 appear. The stretching mode of physisorbed CO_2 is found at 2341 cm^{-1} whereas bands related to the chemical reaction between amino groups and CO_2 are found in the region between 1750 and 1250 cm^{-1}. In order to better appreciate these bands, the spectra are reported after subtraction of the spectrum of the bare sample, *i.e.* before CO_2 admission (Fig. 4B, curves a–a^{IV}). In particular, bands located at 1560, 1482 and 1413 cm^{-1} are associated with the formation of carbamate species and bands at 1692 and 1380 cm^{-1} are attributed to the formation of carbamic acid.[17,32–34] The band at 1625 cm^{-1} is due to the asymmetric bending of NH_3^+ species, probably deriving from the interaction of basic species with carbamic acid,[32] whereas the band at 1310 cm^{-1} is related to skeletal vibrations of $NCOO^-$ species.[35] Further evidence for the formation of carbamic acid is the increase of the large band between 3500 and 2000 cm^{-1} that can be associated with the interaction with NH_2 species at the MCM-41 surface. By decreasing progressively the CO_2 pressure (Fig. 4B, curves a^I–a^{IV}) bands related to carbamates and carbamic acid species progressively decrease in intensity, indicating that part of the reaction products are removed by the outgassing procedure. The adsorption of CO_2 on P_MCM-41 nano (Fig. 4b′) also leads to the formation of physisorbed and chemisorbed species. To compare the results obtained for the two samples in terms of physisorbed species, the difference spectra are reported in Fig. S2 (ESI†).[16] It can be seen that the physisorbed CO_2 is much more abundant in the P_MCM-41 nano sample probably because of its higher pore volume in comparison to P_MCM-41 micro: 0.864 cc g^{-1} and 0.363 cc g^{-1}, respectively (Table 1). Concerning chemisorbed species, it can be seen that bands in the 1750–1250 cm^{-1} range

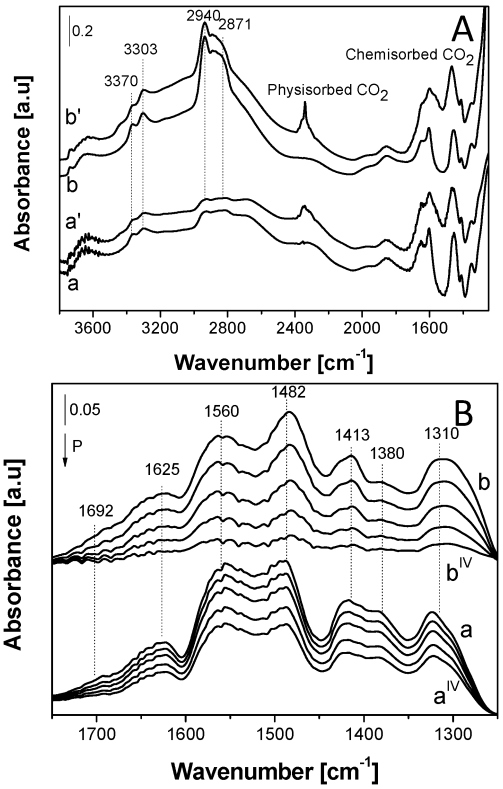

Fig. 4 Section A: FTIR spectra in the 3800–1250 cm^{-1} region of P_MCM-41 micro (a) and P_MCM-41 nano (b) before (curves a and b) and after exposure to 60 mbar of CO_2 at 35 °C (curves a′ and b′). Section B: FTIR spectra, in the 1750–1250 cm^{-1} region, of CO_2 adsorbed (P_{max} = 60 mbar) at 35 °C on P_MCM-41 micro (a–a^{IV}) and P_MCM-41 nano (b–b^{IV}). The arrows indicate decreasing CO_2 pressure until vacuum. Spectra are reported after subtraction of the spectrum recorded before CO_2 interaction, used as a background, and after the subtraction of the spectrum of gaseous CO_2.

(those stable upon evacuation) are more intense for the MCM-41 micro sample with respect to the nano, thus indicating a greater amount of stable carbamates and carbamate acids in the micro-sized sample. The desorption process, in fact, is different for the two samples: in P_MCM-41 nano the bands decrease faster and remain less intense, while in MCM-41 micro the bands decrease less rapidly and remain well visible also at the end of desorption. This is also supported by the fact that the broad band in the 3500–2000 cm^{-1} range upon evacuation is more pronounced for P_MCM-41 micro than for the nanosized sample (see Fig. S3, ESI†), thus suggesting a stronger interaction between the carbamic acid and the basic species at the silica surface. This is probably due to the location of amino groups grafted on the silica surface: in P_MCM-41 nano more amino groups are present on the external surface, outside the pores, and probably the formed carbamates are less protected by confinement effects with respect to P_MCM-41 micro.

Further insight into the nature of the CO_2 adsorption processes is obtained with the use of solid state NMR spectroscopy using the approach of earlier works as reported previously.[17,36,37] The ^{13}C MAS NMR data recorded for P_MCM-41 samples containing $^{13}CO_2$ are presented in Fig. 5.

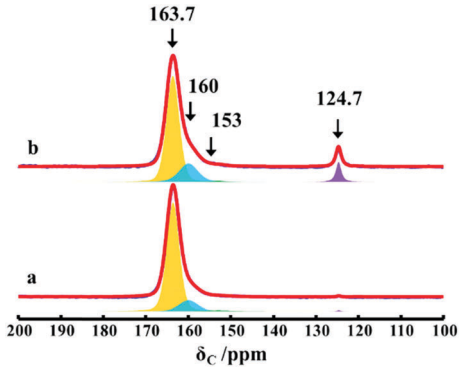

Fig. 5 ^{13}C MAS NMR spectra of $^{13}CO_2$ adsorbed on P_MCM-41 micro (a) and P_MCM-41 nano (b) recoded using a MAS rate of 10 kHz. Each spectrum includes experimental and deconvoluted spectra with individual contributions from each ^{13}C site.

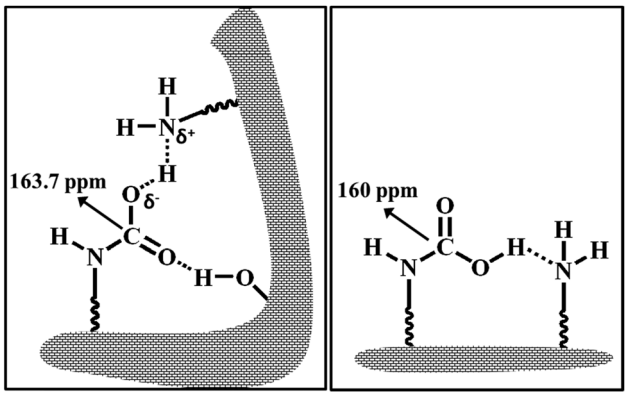

Fig. 6 Schematic diagram representing two possible models of the hydrogen bonding network formed by carbamate and carbamic acid species with surface silanols and neighboring PAPTS units.

Room temperature ^{13}C magic angle spinning NMR spectra of micro and nano P_MCM-41 samples show peaks due to both physisorbed and chemisorbed $^{13}CO_2$ species. The ^{13}C MAS NMR spectra contain one primary isotropic peak at 124.7 ppm, due to physisorbed $^{13}CO_2$. Three additional ^{13}C resonances at 163.7, 160, and 153 ppm, typically associated with carbamate carbons formed upon $^{13}CO_2$ chemisorption with the PAPTS amines, were found. Mafra *et al.* on their study of amine-functionalized SBA-15 have reported that three distinct carbonyl environments involving hydrogen bonding with surface silanols and neighboring alkylamines were responsible for those resonances.[37] Quantitative data derived from the ^{13}C MAS NMR spectra show that around 7% of the total $^{13}CO_2$ was in the form of physisorbed species while the rest is distributed among chemisorbed species in P_MCM-41 nano (Table 2). However, the physisorbed $^{13}CO_2$ present in the P_MCM-41 micro sample was less than 1%. Amongst the three chemisorbed species, the peak at 163.7 ppm contributed 85% of the total carbamate species.

It is clear from the ^{13}C MAS NMR study that the storage capacity and distribution of $^{13}CO_2$ vary in samples according to their pore architecture (topology) and particle dimension. The limited amount of physisorbed $^{13}CO_2$ in the micro sample, in full agreement with the IR findings (*vide supra*), could be due to the reduced porous volume of this sample (0.363 cc g^{-1}) with respect to the nanometric one (0.864 cc g^{-1}, Table 1). In addition, the lower amount of physisorbed $^{13}CO_2$ might also be due to the hydrogen bonded carbamate and/or carbamic acid network blocking the access of gaseous $^{13}CO_2$ to the channels. The hydrogen bonded network configurations formed in these samples are shown in Fig. 6.

Table 2 Quantitative data derived from the 13C MAS NMR spectra of $^{13}CO_2$ adsorbed P_MCM-41

Chemical shift, δ_c [ppm]	P_MCM-41 micro [wt%]	P_MCM-41 nano [wt%]
163.7	85	72
160	13	20
153	<2	1
124.7	<1	7

The peak at 163.7 ppm is formed by a complex hydrogen bonding network involving multiple species that dominates in sample P_MCM-41 micro. Such a complex network could fill the channels as well as block the access for gaseous $^{13}CO_2$. However, in the P_MCM-41 nano sample, not all $^{13}CO_2$ species contribute to the peak at 163.7 ppm. This leaves just enough space for the access of gaseous $^{13}CO_2$ to the channels as seen by the intense peak at 124.7 ppm.

The behavior of an adsorbate ($^{13}CO_2$) trapped within MCM-41 is dictated by both the porous architecture of the solid itself and the interaction with the surface species. The nature of the interaction with $^{13}CO_2$ (physisorbed or chemisorbed) can have a significant effect on their behavior within a porous solid.

Thermogravimetric study of the CO_2 adsorption

The CO_2 adsorption capacity was monitored by TGA performing adsorption/desorption analysis (Fig. 7).

TGA adsorption curves show that P_MCM-41 nano (Fig. 7, curve b) has a higher CO_2 adsorption capacity compared to the P_MCM-41 micro sample (Fig. 7, curve a). Indeed, the CO_2 uptake after 2 h of adsorption is 0.79 and 0.58 mmol g^{-1}, respectively. For both samples, during the adsorption there is a fast initial uptake of CO_2, followed by a second slower process. This is generally an indication of a non-isothermal adsorption process in which molecules are rapidly adsorbed producing a temperature increase and then, as the sample cools down more molecules are slowly adsorbed. This is confirmed by the temperature profile of the samples as well as the heat of adsorption measured by the instrument (Fig. 7, frames B and C). The small variation of the sample temperature (about 0.01 °C) is due to the fact that in this system thermocouples are not placed inside the sample, but in the camera where the crucibles are inserted: for this reason, the registered temperature is an intermediate temperature between the sample and the gas.

The organo-modified silica samples show also different adsorption–desorption rates: P_MCM-41 micro shows a slower adsorption and desorption rate compared to P_MCM-41 nano, suggesting a higher contribution of chemisorption. This is particularly evident in the desorption curve where at the end

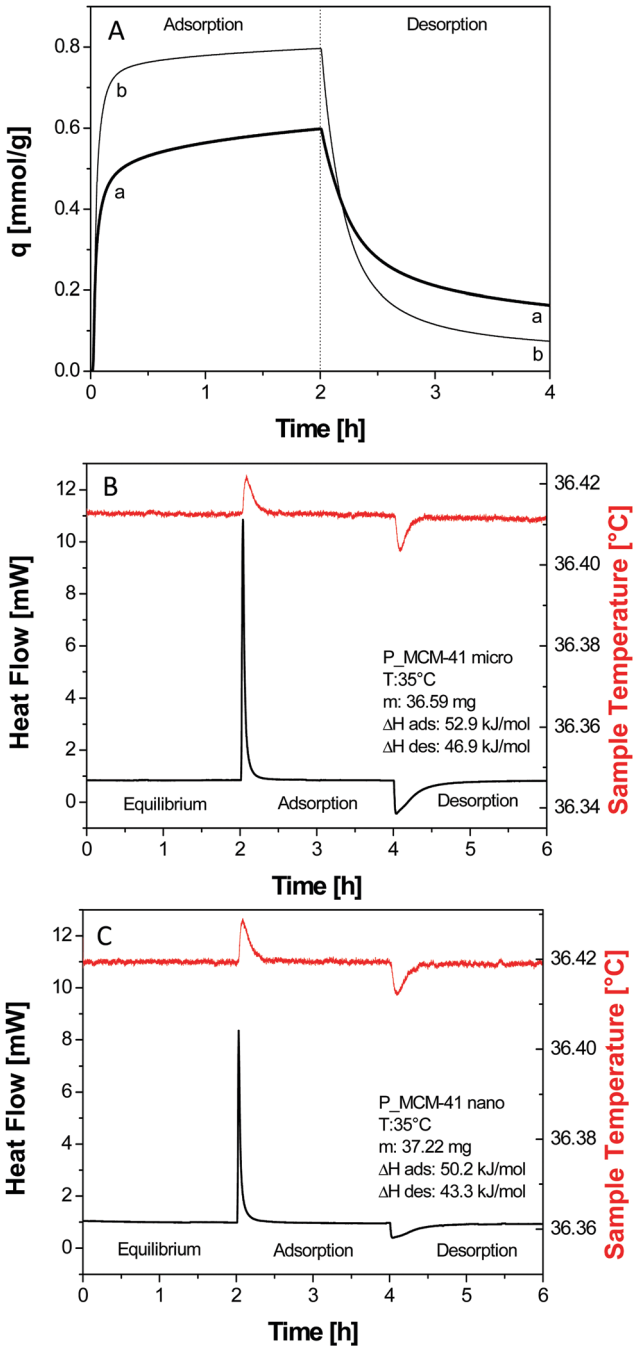

Fig. 7 Frame A: CO_2 uptake curves obtained from TGA analysis of P_MCM-41 micro (a) and P_MCM-41 nano (b) silica samples. Measurements were recorded at 35 °C, 0.1 bar CO_2–0.9 bar He in adsorption and 1 bar He in desorption. Frame B and C: Heat flow and sample temperature from DSC-TGA analysis for P_MCM-41 micro and P_MCM-41 nano samples.

of the 2 h desorption step, despite the lower uptake, a much higher proportion of CO_2 is retained in the micro sample (≈27% of the total) as compared to the nano sample (≈9% of the total). This confirms that P_MCM-41 micro has a higher chemisorbed irreversible fraction, strongly interacting with the surface, as also observed using FT-IR Spectroscopy.

From the TG-DSC analyser the adsorption (ΔH_{Ads}) and desorption heats (ΔH_{Des}) of the process can also be calculated from the heat flow, measured by the DSC using eqn (2), where m is the amount of adsorbed CO_2 in moles and t is the time.[2]

$$\Delta H = \frac{\int_{t_0}^{t} \text{Heat flow d}t}{m_t - m_{t_0}} \quad (2)$$

Eqn (2): Adsorption and desorption heats of the process.

The calculated values of ΔH_{Ads} and ΔH_{Des} are in agreement with that observed for the amount adsorbed. The ΔH_{Ads} values for P_MCM-41 micro and P_MCM-41 nano samples are 52.9 and 50.2 kJ mol^{-1}, respectively; while the corresponding ΔH_{Des} values are lower (46.9 kJ mol^{-1} and 43.3 kJ mol^{-1}, respectively). The lower heat associated with the desorption process indicates that the amount desorbed is primarily the fraction physisorbed of the total adsorbed amount. These data are also observable in Fig. 7B and C: the adsorption heat (*i.e.* the area under the Heat Flow) is greater with respect to the desorption heat, thus indicating that during the desorption mainly physisorption occurred. In the literature, processes with ΔH values lower than 50 kJ mol^{-1} are considered to be physisorption, while values greater than 50 kJ mol^{-1} are considered to be chemisorption.[38] In this case, both samples have adsorption heats corresponding to the limit value (50 kJ mol^{-1}), suggesting that both physisorption and chemisorption processes are present. It is worth noting that the adsorption heats for the pristine samples (before the grafting procedure) were 37.1 and 37.9 kJ mol^{-1} for MCM-41 micro and MCM-41 nano samples, respectively (Fig. S4, ESI†). In these materials only physisorption can occur, because amino groups, which can react chemically with the CO_2, are not present. It is clear then that the increase in the ΔH_{Ads} for the P_MCM-41 micro and nano samples is due to the contribution of the chemisorption associated with the amino groups added.

The adsorption of CO_2 was also studied using ZLC analysis to determine quantitatively the reversible fraction of CO_2 uptake at 35 °C. Fig. 8 shows the ZLC desorption curves of the P_MCM-41 micro sample (section A) and the P_MCM-41 nano sample (section B) at different flow rates: 2 and 2.7 ml min^{-1}; the plots include the blank curves (*i.e.* the response of the system when no sample is loaded). In this plot the *x*-axis is the product of the flow rate of the carrier (He) and the time, *i.e.* the volume of gas eluted. It is then clear that the difference between the area under the desorption curve of the sample and the blank is proportional to the amount of adsorbed CO_2. Consequently, applying a mass balance on the column, the uptake can be calculated by integration of the obtained signals.[38]

The calculated values of CO_2 capacity are: 0.349 and 0.58 mmol g^{-1} for P_MCM-41 micro and P_MCM-41 nano respectively. These capacity values are significantly lower than those obtained with TGA. This is due to the fact that the ZLC method measures the amount of CO_2 desorbed from the sample. For a purely physisorption process it is expected that this value is the same as the amount originally adsorbed on the sample. In our case instead, a portion of CO_2 is chemically

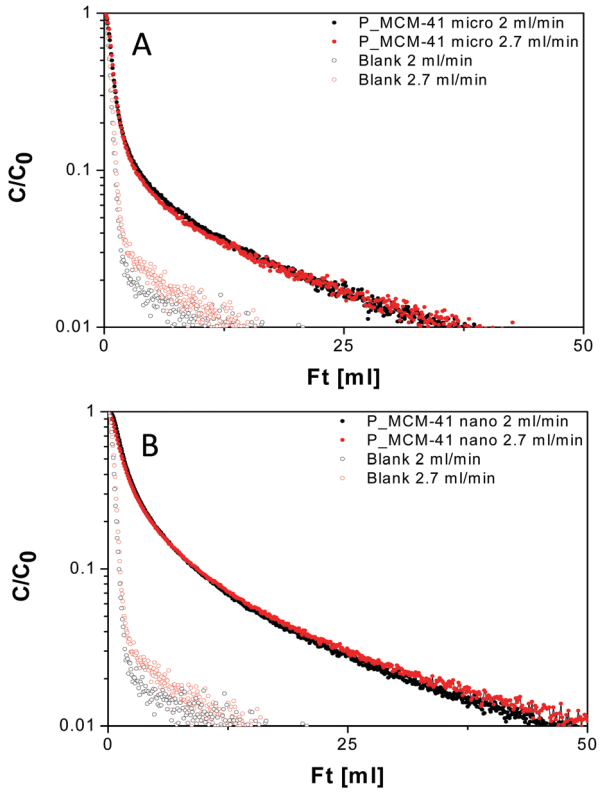

Fig. 8 ZLC desorption curves of P_MCM-41 micro (section A) and P_MCM-41 nano samples (section B) and blank curves at 2 and 2.7 ml min^{-1} flow rates. CO_2 partial pressure: 0.1 bar, *T*: 35 °C.

bound to the amine groups, and therefore irreversibly adsorbed during the time of the experiment. Indeed, an irreversible chemisorbed fraction has already been observed by FT-IR spectroscopy and TGA analysis.

In order to desorb also the irreversible fraction, and obtain the total adsorption capacity, temperature programmed desorption (TPD) analysis was carried out on P_MCM-41 samples. The obtained TPD curves are reported in Fig. S5 (ESI†). The obtained values of irreversible fractions respectively for P_MCM-41 micro and P_MCM-41 nano samples are 0.16 and 0.06 mmol g^{-1}, respectively. Taking into account the amount of irreversible fraction observed with TPD, a more accurate value of CO_2 adsorption capacity can be obtained: 0.51 and 0.64 mmol g^{-1} for the P_MCM-41 micro and P_MCM-41 nano samples, respectively. These data are now only slightly lower than the capacity values obtained *via* volumetric and thermogravimetric analysis. The ZLC experiment was in fact the last experiment carried out in the samples, for this reason it was suspected that the loss of capacity could be associated with the degradation of the samples. For this reason a new TGA measurement was carried out on the same nano sample used to pack the ZLC. The new measured capacity was 0.63 mmol g^{-1} for the P_MCM-41 nano sample, confirming that the discrepancy in the values observed in the ZLC experiment is due to degradation of the samples. Furthermore, the fraction of chemically adsorbed CO_2 in ZLC analysis accounts for about 31 and 9% of the total adsorbed, which is in very good agreement with what was observed in the gravimetric experiment. In Table 3 the values of adsorption capacities obtained with ZLC, TGA and volumetric analysis are summarized.

Table 3 Adsorption capacity values obtained with thermogravimetric analysis, volumetric analysis and zero length column chromatography

	Adsorption capacity [mmol g^{-1}]		
Sample	TGA	Volumetry	ZLC
P_MCM-41 micro	0.58	0.62	0.51
P_MCM-41 nano	0.79	0.79	0.64

Temperature dependence of the CO_2 adsorption process

In order to study the temperature dependence of the CO_2 adsorption on hybrid MCM-41 materials, we performed *in situ* FT-IR spectroscopy at different temperatures (35, 50, 70 and 90 °C). The spectra obtained in the 1750–1250 cm^{-1} region are reported in Fig. 9. When the temperature increases from 35 to 90 °C, the bands due to ammonium carbamates and carbamic acid decrease in intensity, and this is especially evident for the P_MCM-41 nano sample. In fact, the products resulting from the reaction between CO_2 and the NH_2 groups are thermally unstable upon heating.[3] This is in agreement with previous studies, which demonstrated that carbon dioxide started to be desorbed above 40 °C.[39] The fact that the products formed on P_MCM-41 micro show a greater stability compared to the P_MCM-41 nano sample with the increase of the temperature suggests that in the micrometric sample the organic chains, and thus the formed products, are located mainly inside the pores where they are confined and more protected toward decomposition/desorption.

The temperature dependence of the CO_2 adsorption process was also studied using the gravimetric method. Fig. 10 (sections A and B) shows the uptake of CO_2 as a function of temperature (20–90 °C) for the organo-modified MCM-41 silica samples.

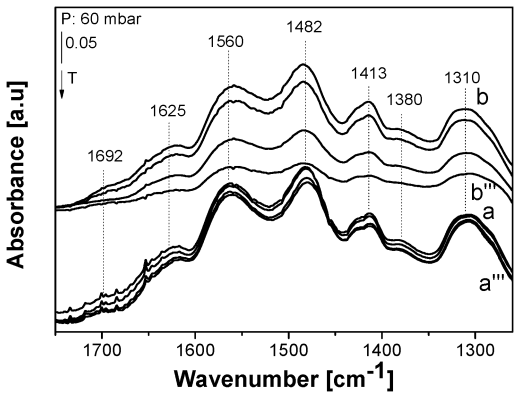

Fig. 9 FTIR spectra, in the 1750–1250 cm^{-1} region of P_MCM-41 micro (curves a–a^{III}) and P_MCM-41 nano (curves b–b^{III}) after the admission of 60 mbar of CO_2. The arrows indicate increasing temperature 35, 50, 70 and 90 °C. Spectra are reported after subtraction of the spectrum recorded before CO_2 interaction, and the subtraction of the spectrum of the CO_2 gas.

The gas uptake after 2 h of adsorption decreases with the increase of the temperature.[16,40] This behavior is evident in both samples, but for the P_MCM-41 micro sample the decrease is less pronounced, confirming FT-IR observations. For both MCM-41 hybrid samples, increasing the temperature decreases the residual amount of chemisorbed CO_2. However, the stability of such species is different: for P_MCM-41 nano at 90 °C there is not a CO_2 residual fraction, while for the P_MCM-41 sample at 90 °C 6.7% of adsorbed CO_2 is still present. The adsorbed and desorbed amounts of CO_2 (reversible and irreversible fractions) are summarized in Table S2 in the ESI.†

Even if the CO_2 uptake decreases when the temperature increases, the overall heat of adsorption increases to 70.3 and 66.5 kJ mol^{-1} at 90 °C for P_MCM-41 micro and P_MCM-41 nano samples (Fig. 10, section C), respectively. The higher ΔH_{ads} is probably related to the fact that by increasing the temperature the physisorption process no longer plays a significant role. Thus, the measured ΔH_{ads} value approaches the one of the pure chemisorption process.[41]

The temperature-dependence of the CO_2 uptake was also studied using a volumetric adsorption analyzer. Fig. 11 shows the experiments at 35 and 50 °C for both the MCM-41 grafted samples. Fig. 11 shows that P_MCM-41 nano has a higher CO_2 adsorption capacity at 35 °C compared to the P_MCM-41 micro sample: at a relative pressure comparable with TGA analysis and post combustion conditions (p = 100 mbar) the CO_2 uptake values are 0.79 and 0.62 mmol g^{-1}, respectively, in agreement with the CO_2 uptake values obtained with TGA (0.79 and 0.58 mmol g^{-1}). However, the isotherms of the two P_MCM-41 samples show different shapes. For the P_MCM-41 nano curve, the volume of adsorbed CO_2 continues to rise by increasing the pressure, being, in the range of pressures considered, far from saturation. Conversely, the P_MCM-41 micro sample presents an isotherm with a quasi-rectangular shape, which is steeper than that of P_MCM-41 at low pressure, indicating the presence of stronger adsorption sites accounting almost entirely for the total capacity of the sample. The sample approaches its saturation capacity already at atmospheric pressure.

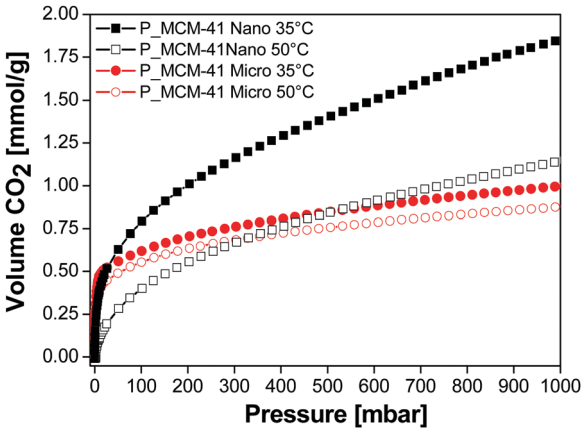

Fig. 11 CO_2 uptake of P_MCM-41 micro and P_MCM-41 nano samples at 35 and 50 °C obtained by volumetric measurements.

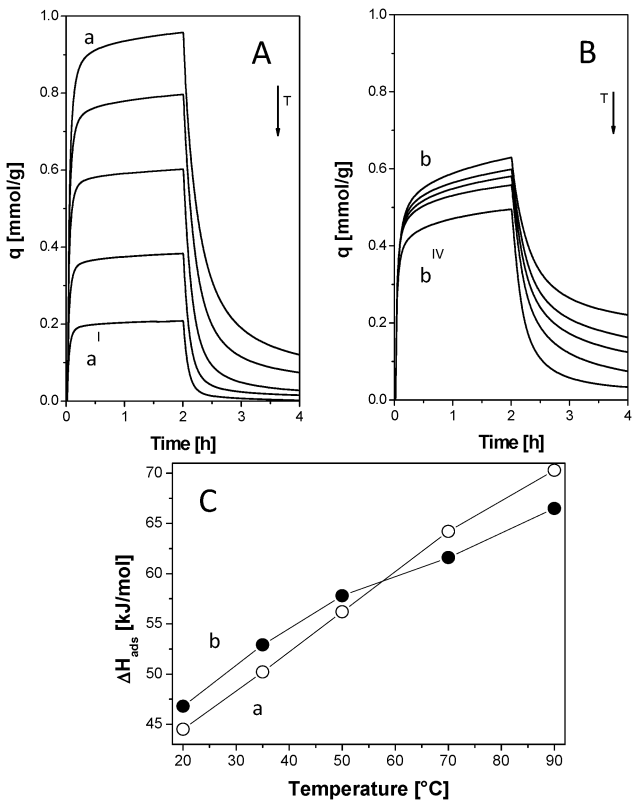

Fig. 10 CO_2 uptake curves obtained with TGA analysis of P_MCM-41 nano (section A) and P_MCM-41 micro (section B) samples at 20, 35, 50, 70 and 90 °C (a to a^{IV} and b to b^{IV} curves). Section C: Adsorption heat at different temperatures for P_MCM-41 micro (a) and P_MCM-41 nano (b) samples.

For both samples, the uptake of CO_2 decreases with the increase of the temperature. However, this behavior for the P_MCM-41 sample is less pronounced than for the P_MCM-41 nano sample, thus fully confirming the observations obtained with TGA analysis.

Conclusions

In this work the CO_2 adsorption properties of organo-modified MCM-41 were studied. A combination of FTIR and SS-NMR spectroscopies provided information on the physisorption and chemisorption interactions between CO_2 and the hybrid solids. This approach revealed that a higher amount of physisorbed CO_2 is present in the nanometric MCM-41 sample compared to the micrometric one essentially because of a higher pore volume. The amount of carbon dioxide adsorbed on hybrid MCM-41 was determined by three different quantitative techniques: gravimetric analysis, Zero Length Column chromatography and volumetric analysis. The obtained values of the CO_2 adsorption capacity, for P_MCM-41 nano and P_MCM-41 micro, are respectively: 0.79 and 0.58 mol kg^{-1} (TGA), 0.64 and 0.51 mol kg^{-1} (ZLC) and 0.79 and 0.62 mol kg^{-1} (volumetric analysis). In addition, the reversibility of the reaction was investigated. After 2 h of desorption, the micrometric sample shows a residual

amount of chemisorbed CO_2 higher than the nanometric sample (respectively 27% and 9% of the total adsorbed CO_2).

Finally, the adsorption process was studied at different temperatures in order to find the best operating conditions. For both samples, on increasing the temperature from 35 to 90 °C, the amount of adsorbed carbon dioxide decreases, as expected for an exothermic process. For this reason, the best conditions in terms of working capacity for our samples have been found at 35 °C. The carbamate products resulting from the reaction between CO_2 and the amino groups are thermally unstable and release CO_2 upon heating. However, the carbamate products in the micrometric sample show a greater stability, compared to those in the nanometric one, because of the protection by the pores, which provide a larger quantity of confined species.

Conflicts of interest

There are no conflicts to declare.

Acknowledgements

The authors are fully grateful to Mrs Chiara Zaccone for her help in the physico-chemical characterization of the porous samples and to Dr Claudio Evangelisti (ISTM-CNR, Milan) for TEM measurements. The authors also acknowledge the financial support by the Italian Ministry of Education, University and Scientific Research (MIUR) through the PRIN Project 2010A2FSS9.

Notes and references

1 S. D. Kenarsari, D. Yang, G. Jiang, S. Zhang, J. Wang, A. G. Russell, Q. Weif and M. Fan, *RSC Adv.*, 2013, **3**, 22739–22773.
2 M. E. Boot-Handford, J. C. Abanades, E. J. Anthony, M. J. Blunt, S. Brandani, N. Mac Dowell, J. R. Fernàndez, M.-C. FerrarI, R. Gross, J. P. Hallett, R. S. Haszeldine, P. Heptonstall, A. Lyngfelt, Z. Makuch, E. Mangano, R. T. J. Porter, M. Pourkashanian, G. T. Rochelle, N. Shah, J. G. Yao and P. S. Fennell, *Energy Environ. Sci.*, 2014, **7**, 130–189.
3 B. Dutcher, M. Fan and A. G. Russell, *ACS Appl. Mater. Interfaces*, 2015, **7**, 2137–2148.
4 S. Choi, J. H. Drese and C. W. Jones, *ChemSusChem*, 2009, **2**, 796–854.
5 A.-H. Lu and G.-P. Hao, *Annu. Rep. Prog. Chem., Sect. A: Inorg. Chem.*, 2013, **109**, 484–503.
6 R. Ben-Mansour, M. A. HabiB, O. E. Bamidele, M. Basha, N. A. A. Qasem, A. Peedikakkal, T. Laoui and M. Ali, *Appl. Energy*, 2016, **161**, 225–255.
7 X. Xu, C. Song, J. M. Andresen, B. G. Miller and A. W. Scaroni, *Energy Fuels*, 2002, **16**, 1463–1469.
8 C.-J. Yoo, L.-C. Lee and C. W. Jones, *Langmuir*, 2015, **31**, 13350–13360.
9 Y. Belmabkhout and A. Sayari, *Adsorption*, 2009, **15**, 318–328.
10 Y. Belmabkhout, G. De Weireld and A. Sayari, *Langmuir*, 2009, **25**, 13275–13278.
11 Y. Belmabkhout, R. Serna-Guerrero and A. Sayari, *Chem. Eng. Sci.*, 2010, **65**, 3695–3698.
12 Y. Belmabkhout, R. Serna-Guerrero and A. Sayari, *Chem. Eng. Sci.*, 2009, **64**, 3721–3728.
13 C. Chen, J. Kim and W.-S. Ahn, *Korean J. Chem. Eng.*, 2014, **31**, 1919–1934.
14 X. Xu, C. Song, J. M. Andresen, B. G. Miller and A. W. Scaroni, *Energy Fuels*, 2002, **16**, 1463–1469.
15 J. C. Hicks, J. H. Drese, D. J. Fauth, M. L. Gray, G. Qi and C. W. Jones, *J. Am. Chem. Soc.*, 2008, **130**, 2902–2903.
16 Z. Bacsik, R. Atluri, A. E. Garcia-Bennett and N. Hedin, *Langmuir*, 2010, **26**, 10013–10024.
17 G. Gatti, D. Costenaro, C. Vittoni, G. Paul, V. Crocellà, E. Mangano, S. Brandani, S. Bordiga, M. Cossi, C. Bisio and L. Marchese, *Phys. Chem. Chem. Phys.*, 2017, **19**, 14114–14128.
18 N. N. A. H. Meis, J. H. Bitter and K. P. de Jong, *Ind. Eng. Chem. Res.*, 2010, **49**, 1229.
19 P. Galhotra, J. G. Navea, S. C. Larsena and V. H. Grassian, *Energy Environ. Sci.*, 2009, **2**, 401–409.
20 J. S. Beck, J. C. Vartuli, W. J. Roth, M. E. Leonowicz, C. T. Kresge, K. D. Schmitt, C. T.-W. Chu, D. H. Olson, E. W. Sheppard, S. B. McCullen, J. B. Higgins and J. L. Schlenkert, *J. Am. Chem. Soc.*, 1992, **114**, 10834–10843.
21 K. Suzuki, K. Ikari and H. Imai, *J. Am. Chem. Soc.*, 2004, **126**, 462–463.
22 L. Etgar, G. Schuchardt, D. Costenaro, F. Carniato, C. Bisio, S. M. Zakeeruddin, M. K. Nazeeruddin, L. Marchese and M. Graetzel, *J. Mater. Chem. A*, 2013, **1**, 10142–10147.
23 J. A. A. Gibson, A. V. Gromov, S. Brandani and E. E. B. Campbell, *Microporous Mesoporous Mater.*, 2015, **208**, 129–139.
24 X. Hu, S. Brandani, A. I. Benin and R. R. Willis, *Ind. Eng. Chem. Res.*, 2015, **54**, 6772–6780.
25 S. Brandani and D. M. Ruthven, *Adsorption*, 1996, **2**, 133–143.
26 F. Brandani, D. Ruthven and C. G. Coe, *Ind. Eng. Chem. Res.*, 2003, **42**, 1451–1461.
27 D. Massiot, F. Fayon, M. Capron, I. King, S. Le Calve, B. Alonso, J.-O. Durand, B. Bujoli, Z. Gan and G. Hoatson, *Magn. Reson. Chem.*, 2002, **40**, 70–75.
28 C. Vittoni, V. Sacchetto, D. Costenaro, S. Mastroianni, A. Hinsch, L. Marchese and C. Bisio, *Sol. Energy*, 2016, **124**, 101–113.
29 S. Lowell, J. E. Shields, M. A. Thomas and M. Thommes, *Characterization of Porous Solids and Powders: Surface Area, Pore Size and Density*, Kluwer Academic Publishers, 2004.
30 G. Socrates, *Infrared and Raman Characteristic Group Frequencies*, John Wilway & Sons, Ltd, 2001.
31 C.-Y. Chen, H.-Y. Li and M. E. Davis, *Microporous Mater.*, 1993, **2**, 17–26.
32 X. Wang, W. Schwartz, J. C. Clark, X. Ma, S. H. Overbury, X. Xu and C. Song, *J. Phys. Chem. C*, 2009, **113**, 7260–7268.
33 A. Danon, P. C. Stair and E. Weitz, *J. Phys. Chem. C*, 2011, **115**, 11540–11549.
34 S. A. Didas, M. A. Sakwa-Novak, G. S. Foo, C. Sievers and C. W. Jones, *J. Phys. Chem. Lett.*, 2014, **5**, 4194–4200.

35 C. Knofel, C. Martin, V. Hornebecq and P. L. Llewellyn, *J. Phys. Chem. C*, 2009, **113**, 21726–21734.
36 M. L. Pinto, L. Mafra, J. M. Guil, J. Pires and J. Rocha, *Chem. Mater.*, 2011, **23**, 1387–1395.
37 L. Mafra, T. Čendak, S. Schneider, P. V. Wiper, J. Pires, J. R. B. Gomes and M. L. Pinto, *J. Am. Chem. Soc.*, 2017, **139**, 389–408.
38 J. A. A. Gibson, E. Mangano, E. Shiko, A. G. Greenaway, A. V. Gromov, M. Lozinska, D. Friedrich, E. E. B. Campbell, P. A. Wright and S. Brandani, *Ind. Eng. Chem. Res.*, 2016, **55**, 3840–3851.
39 O. Leal, C. Bolivar, C. Ovalles, J. J. Garcia and Y. Espidel, *Inorg. Chim. Acta*, 1995, **240**, 183–189.
40 Y. Belmabkhout and A. Sayari, *Adsorption*, 2009, **15**, 318–328.
41 G. P. Knowles, S. W. Delaney and A. L. Chaffee, *Ind. Eng. Chem. Res.*, 2006, **45**, 2626–2633.

